The Impact of Azimuthal Anisotropy on Seismic AVO and Petrophysical Response in a Fractured Wabamun Gas Reservoir

Brian Rex*, Bill Goodway, Cathy Martin, Gordon Uswak
EnCana Corporation, 204-1170 Memorial Dr, NW, Calgary, AB, T2N 3E5
brian.rex@encana.com

ABSTRACT

The evaluation of many fractured carbonate reservoirs would benefit greatly from a reliable method of determining fracture density and orientation from seismic data. Although the most technically exhaustive approach would likely involve multi-component analysis, the potential of azimuthal information contained within conventional AVO must not be overlooked. The focus of this study is a prolific gas well drilled on a dipping seismic reflector at the 7-11-60-03W6 Resthaven prospect in the Smokey sub-basin of north-west Alberta. The regional setting allows for a low angle fault to ramp up-section through the Wabamun limestone. Near vertical fractures cause a strongly anisotropic HTI interval in the footwall of the thrust. This study employs an AVO approach to define the extent of the HTI interval and propose methods to map the bounds of the fractured reservoir.

Data acquisition incorporated a "swath style" geometry resulting in 4 swath lines between five lines with conventional 2D geometry. During the initial interpretation, it was immediately apparent that the amplitudes of reflections within the fracture zone are stronger on the swath data than on the conventional data. Although ray path geometry for swath data may not be immediately intuitive, the nearest available offsets contain information from an azimuth normal to the recording line (in this case, along fracture strike). The anomalous amplitudes are attributed to the azimuthal variations in the AVO gradient as dictated by the anisotropy.

A simplified two-layer reservoir model is proposed using surface seismic and some convincing petrophysical evidence. The reservoir model consists of a shear fault zone consisting of sub-horizontal fractures (VTI) juxtaposed with a vertically fractured footwall (HTI). Evidence of shear wave birefringence in the full waveform sonic log and polarization horns on the resistivity log were the keys in verifying the occurrence of vertical tension fractures in the HTI interval. Ruger (1998) proposed that birefringence ($\Delta\gamma$) is a primary factor in the magnitude of observed azimuthal anisotropy. The results of this AVO study validate the potential for Ruger's AVO expression to predict and interpret azimuthal anomalies.

For completeness, this study entertains the potential for LMR ($\lambda\mu\rho$) analysis. LMR style analysis was intended for application in a near isotropic environment, yet is robust in a variety of anisotropic environments. Applying an LMR approach at Resthaven required some reworking of the isotropic definitions of

$\lambda\mu\rho$. This is done by evaluating the local relationships between $\lambda\mu\rho$ and the in-situ HTI environment as derived from petrophysics.

Local Structural Setting

The model for the origin of the Wabamun shear zone is related to differences in response to Laramide regional stress between the Wabamun carbonate and Ireton shale. The Ireton shale basin responded to Laramide compressional stresses by porosity reduction and dewatering during pressure solution. As the shales pinched out against a Leduc margin to the east, the fluid movement and overpressuring was directed upward against the more brittle and relatively impermeable Wabamun. Elevated pore fluid pressures above the Ireton shale basin combined with Laramide compressional stresses induced both local shear failure and shortening of the more brittle Wabamun carbonate, as well as more widespread vertical tension fractures.
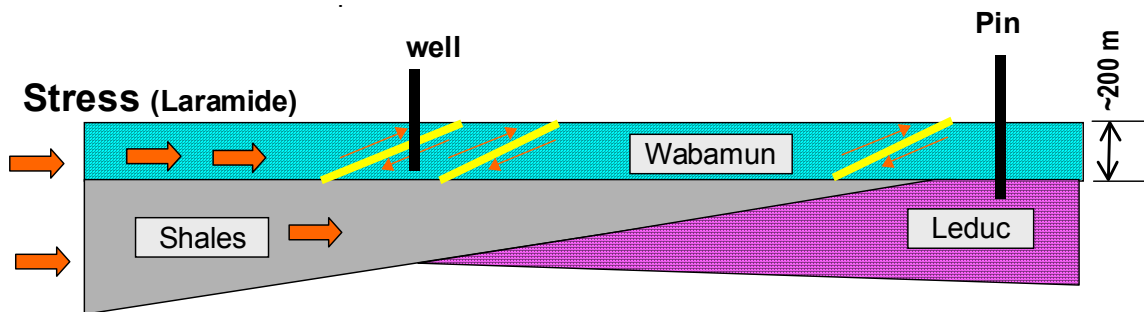
Fig. 1:Schematic of Wabamun Fracture Origins. Stress in the Wabamun and shales, reduces porosity, increases pore fluid pressure, thereby reducing effective stress in the Wabamun. This leads to shear failure, tension fractures and overpressure (M.Warren & M. Cooper, Encana Corp).

The brittle deformation in the shear zones (figure 2) manifests itself as a zone of deformation, rather than a single fault surface. The deformation zone consists of a series of sub-horizontal or gently dipping fractures and small-scale faults dipping toward the main thrust front.
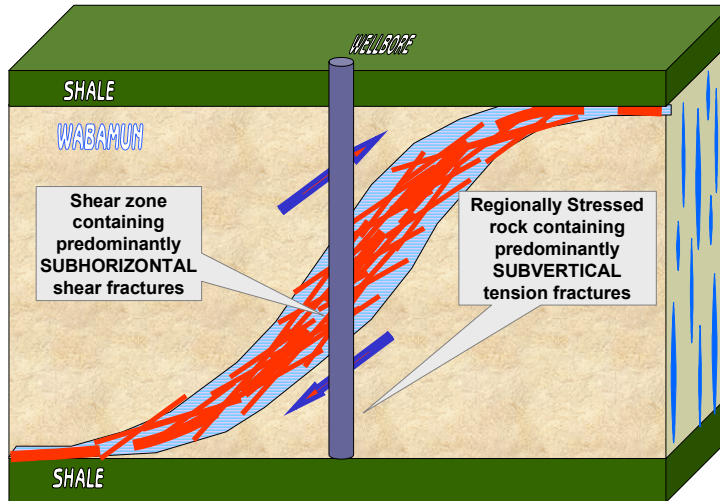
Fig. 2: Schematic of Shear Zone. The shear zone consists of sub-horizontal shear fractures that are bound above and below by the sub-vertical tension fractures of the regionally stressed rock.

Data Collection

With consideration for sensitive surface conditions, a 2D swath geometry was deployed. In this geometry, shots along each line are also recorded by the geophones of an adjacent 2D line. The result is a series of swath lines, binned during processing into CMP positions between the shot and recording line. For example, in the figure below, the shots from line 02 (red) were recorded into the geophones of line 06 (red) to create swath line 02-06 (green). Line 4|3 (red, dashed) is an exception where only a line of geophones was deployed to record sources from both lines 4 and 3.

Fig. 3: Acquisition Geometry. Swath data (green) binned into CMP strips between the lines of conventional geometry (red).

3

An obvious result of this geometry is the absence of near offset information in swath data. Furthermore, ray path geometry (figure 4) suggests that the nearest available offsets contain information from wavefronts propagating orthogonal to the line, along the direction of fracture strike. Recognizing the potential impact of this geometry was the key in identifying the azimuthal AVO response of the reservoir.
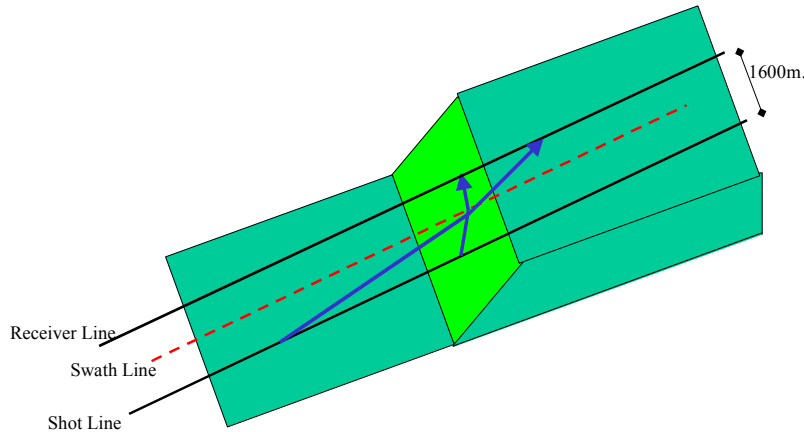
Fig. 4: Schematic of raypath geometry at the footwall. At the nearest available offsets, the swath data contains raypath information oriented along fault & fracture strike.

Data Analysis

There is a notable difference in the reflection strength of the shear zone on conventional and swath lines.
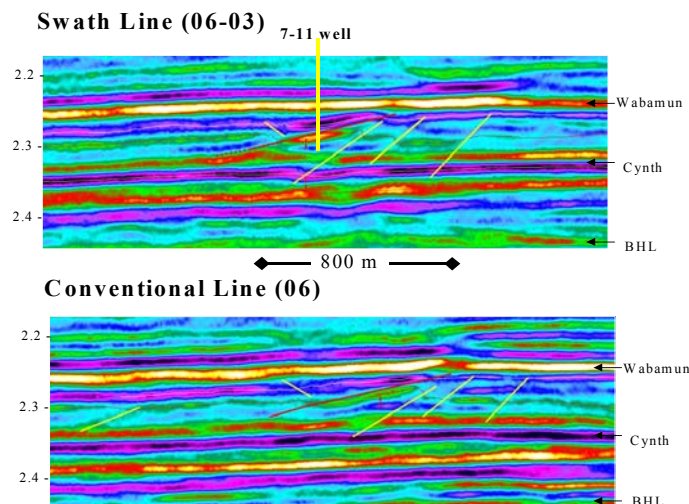
Fig. 5: Seismic cross sections from conventional and swath data. The amplitude of the shear zone reflection is much greater on the swath line. Note: both of these lines have the same source points but were recorded at separate receiver lines.

Two possible causes of the strong reflection amplitudes on the swath data are:
1) an improvement in data quality caused by the absence of near offsets or 2) an azimuthal influence on the amplitude of the shear zone. The gathers (figure 6) contain only minor evidence of near offset noise that is unlikely to deteriorate the stacked response of the conventional data. The impact of changing azimuth is more likely the cause of the swath line anomaly as the swath gather shows a strong offset contribution at the nearest available offsets (1600-2000m). Raypath geometry (figure 4) suggests that this near offset anomaly is generated by a wavefield propogating along fracture strike.

CDP Gather from Conventional line

CDP Gather from Swath line
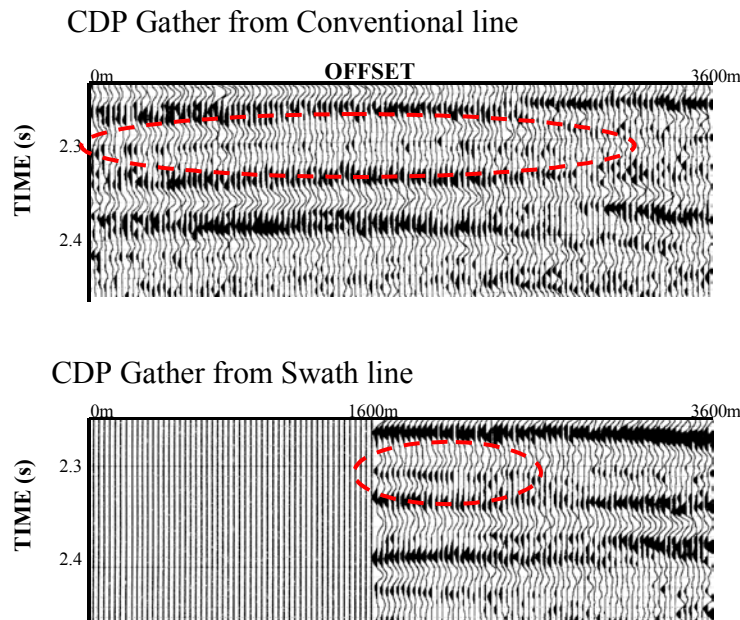
Fig. 6: CMP gathers from conventional and swath data. The major contribution to the stacked amplitude of the swath data is generated at the 1600-2000m offset. This offset range contains information from raypaths at high azimuthal angles to the recording line. This suggests a strong azimuthal AVO influence.

The ability to reliably predict azimuthal AVO is of paramount importance if seismic is to be used to develop fractured reservoirs. Ruger (1998) defines the near offset P-wave reflection coefficient (Rp) as a function of incidence angle (θ) and azimuth (ϕ).
(equation 1.1):

$$Rp(\theta, \phi) = \tfrac{1}{2}\,\Delta z/z \;+\; \tfrac{1}{2}\,B(\phi_k)\sin^2(\theta) \;+\; C(\phi_k)\sin(\theta)^2\tan(\theta)^2$$

After applying the small angle assumption, the impact of the third term becomes negligable and the expression simplifies to a two term solution. Moreover, at offsets large enough that the impact of the C term is appreciable, the AVO is more complicated than elliptical and the data are probably insufficient to analyse it. (Thomsen 2002)

The anisotropic AVO gradient term $B(\phi_k)$ varies as a function of the squared cosine of the azimuthal angle (ϕ).
(equation 1.2):

$$B(\phi_k) = B_{iso} + B_{ani}\cos^2 (\phi_k - \phi_{sym})$$

with, $B_{iso} = \frac{1}{2}(\Delta\alpha/\alpha - (2\beta/\alpha)^2 \Delta G/G)$
and, $B_{ani} = \frac{1}{2} (\Delta\delta^{(v)} + 2(2\beta/\alpha)^2\Delta\gamma)$

Where:
B – AVO gradient
Z – p impedance
G – shear wave modulus
α – average p-wave velocity
ϕ_k – the kth observed azimuth
ϕ_{sym} – the direction of the symmetry axis

The equation for $B(\phi)$ is non-unique since it has 3 unknowns: B_{iso}, B_{ani} and ϕ_{sym}. A simple rough estimate of ϕ_{sym} with a priori knowledge of the approximate fracture symmetry would satisfy the solution. In this case study, it is assumed that the direction of the symmetry axis is along the fault plane.

The expression for "B_{ani}" shows that the azimuthal variation in the reflection response is a function of the shear wave splitting parameter $\Delta\gamma$ and a new anisotropy parameter $\Delta\delta^{(v)}$. This parameter describes the anisotropy for near vertical propogation in the symmetry planes ($\Delta\delta^{(1)}, \Delta\delta^{(2)}$). (Ruger 1998).

The Azimuthal AVO Model

A full waveform sonic log was acquired at the 7-11 wellbore. Analysis of the raw data resulted in an estimate of shear wave birefringence ($\Delta\gamma$) for the HTI interval. Upon estimating the birefringence, an azimuthal AVO modelling exercise was undertaken to verify the method proposed by Ruger.

To illustrate the principle of shear wave splitting, consider a two layer model (figure 7) composed of a VTI layer (shear zone with sub-horizontal fractures) above an HTI layer (footwall with vertical tension fractures). Within the sub-horizontal fractures of the VTI layer, the S-waves will travel at the same velocity in both polarization directions. Within the vertical tension fractures of the HTI layer, S-waves will become polarized with the faster direction along the fracture plane.
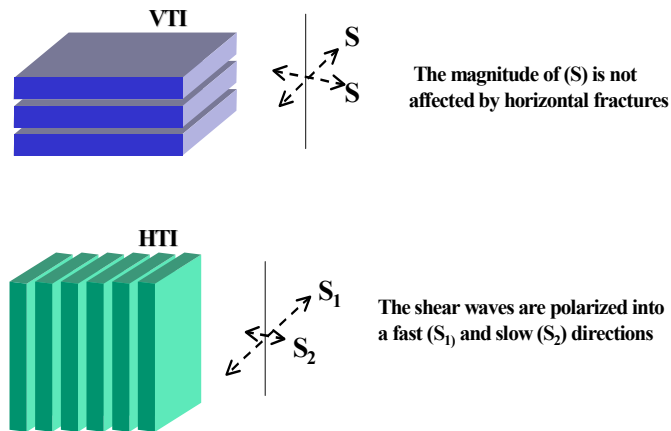
Fig. 7: Schematic of birefringence of vertically propagating shear waves. The vertical tension fractures of the HTI environment initiate polarization of shear waves into fast (along fracture strike) and slow (across fracture strike) directions.

For any given reflector, the first event detected on the full waveform sonic log is the P-reflection followed by the S-reflection and a bevy of high amplitude waves close behind (figure 8). S-wave birefringence within the HTI interval occurs as the outgoing pressure envelope against the fractured borehole is partitioned into fast (S1) and slow (S2) directions. The sonic data used to estimate delay between the two shear modes is recorded at single receiver, located at the farthest offset of the sonic tool. This captured the largest source to receiver travel times and longest separation between the polarized shear modes.
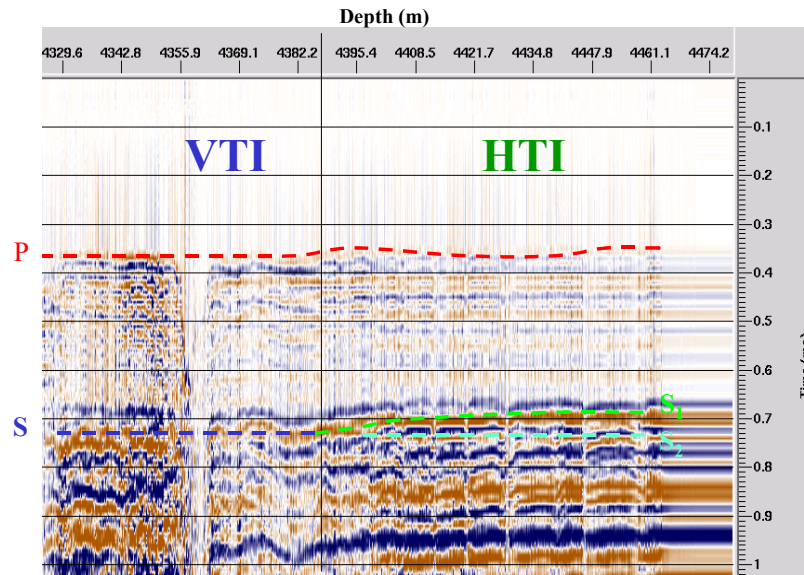
Fig. 8: Full waveform sonic log. The P-wave first arrival (red) shows a slight increase in velocity across the VTI-HTI interface. The S-wave arrival (blue) splits into fast (green) and slow (cyan) polarization directions inside the HTI interval. This waveform is taken from the farthest offset recorder on the sonic tool to allow the most observed delay between the two polarized shear modes (approx. 6% delay).

The delay between the S1 and S2 arrivals suggests a shear wave splitting parameter ($\Delta\gamma$) of approximately 6%. This parameter is believed to be a dominant factor in the magnitude of observed azimuthal anisotropy (Ruger 1998). The following AVA curves (figure 9) illustrate the impact of $\Delta\gamma$ on the predicted azimuthal AVA using the method proposed by Ruger.

Approx to Rugurs solution for AVO in VTI (Gamma 0.066)

Adapted from Ruger 1998
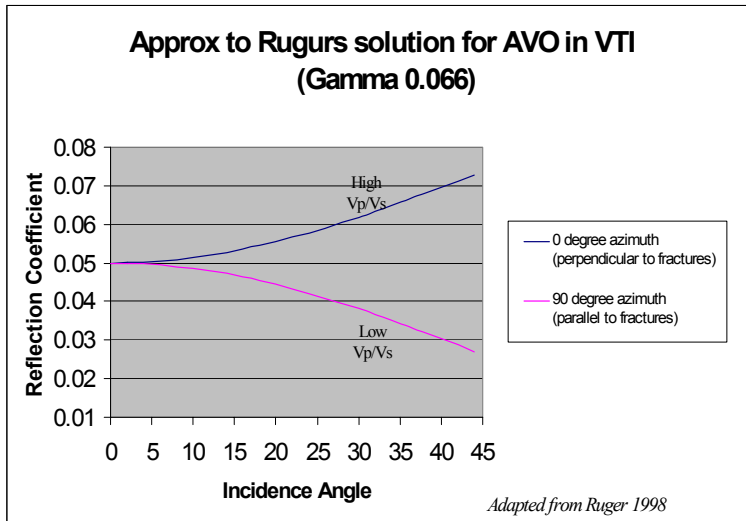
Fig. 9: Calculated Rp vs. Angle (for constant azimuths). The calculated AVO curves indicate that an increasing AVO response is expected along fracture strike and a decreasing AVO response is expected across fractures. The higher shear velocity parallel to fractures results in a lower Vp/Vs ratio in that direction.

These curves represent the predicted AVA at 90 degree azimuth (parallel to fracture strike) and zero degree azimuth (across fracture strike). The calculated AVA for the zero azimuth suggests a decrease in amplitude with angle. This correlates to the observed AVA trend on the conventional gather (figure 6). The calculated AVA curve for the 90 degree azimuth predicts an increase in amplitude with angle. Although the geometry of the swath data (figure 6) only permits recording along fracture strike for a limited range of angles, the strong amplitude at 1600-2000m offset (approx 14^0 to 17^0) suggests that the method is valid as well. It is also reasonable to assume (given no scaling artefacts) that the amplitude of both gathers would be the same at zero incidence.

LMR ($\lambda\mu\rho$) Analysis

Although the LMR method was designed for near isotropic environments it has been applied with surprising effectiveness to anisotropic environments. This section is intended to exhaust the potential for AVO and test the robustness of the LMR method in this obviously anisotropic study area.

One can try to fit the LMR model to satisfy the HTI model by incorporating the effect of vertical fractures on the definitions of the physical parameters. It must be understood why the isotropic parameters for rigidity (μ) and resistance to compression (λ) change as they are measured between a VTI and an HTI environment. To explain these relationships we again refer to the two layer model.

9

$$V_s = \sqrt{\dfrac{\mu}{\rho}}$$

VTI

$\mu = \mu$

HTI

$\mu_1 > \mu_2$
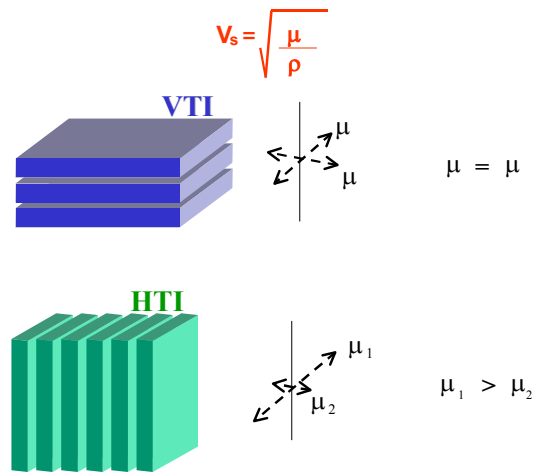
Fig. 10: Schematic of S-wave Propogation. The rigidity (μ) of the HTI interval is governed by the orientation of the tension fractures. The difference in rigidity parallel vs. perpendicular to fractures is largely responsible for the variation in shear velocity.

For the shear wave case it is intuitive that there will be changes in the rigidity modulus between the VTI (μ) and in the HTI (μ_1, μ_2) environment. The first recorded shear arrival (S1), identified as the "s-wave sonic curve, is observed to increase because of the increase in rigidity from VTI (μ) to the HTI (μ_1). If the slower shear arrival (S2) could be identified in log processing we would have an additional shear wave log that decreases across the interface because of the decrease in rigidity from VTI (μ) to the HTI (μ_2). This is an important distinction to recognise when analysing the upcoming petrophysical cross-plot results.

The P-wave case is slightly more complicated since the expression for P-wave velocity (Vp) is composed of both isotropic parameters (λ and μ). As addressed in figure 10, the rigidity (μ) decreases across the interface but it is less intuitive why lambda is observed to increase (figure 11). An explanation for the compressibility change is that the horizontal beds of the upper layer are bound laterally. This will cause the formation to resist vertical compression and results in a relatively high incompressibility. Since the vertical fractures of the lower layer are not bound laterally, they accommodate the expansion of the formation during compression. This will result in a relatively low incompressibility for the lower HTI layer.

$$V_p = \sqrt{\frac{\lambda + 2\mu}{\rho}}$$

Vertical Incompressability (λ) is higher when the medium is "bound laterally"

Vertical Incompressability (λ) is lower as fractures accommodate expansion
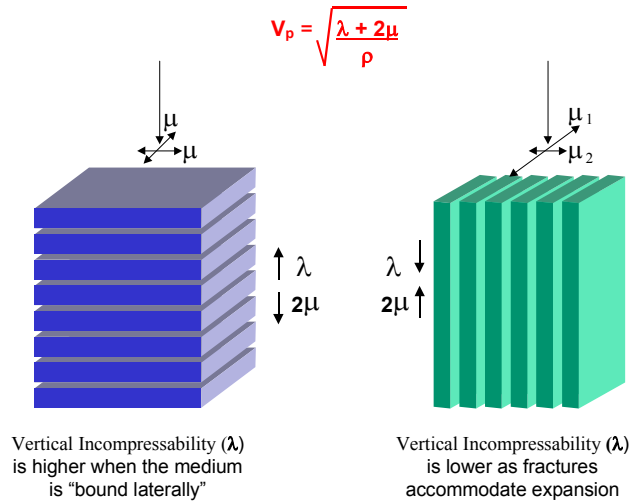
Fig. 11: Schematic of P-wave Propagation. The vertical incompressability (λ) is lower in the HTI layer because the vertical tension fractures accommodate lateral expansion.

Since the relative change on λ and μ are opposite in magnitude, there is little difference in the P-wave velocity across the interface.

To verify the expected LMR behaviour, a template is created by arithmetically manipulating the sonic and density logs from the 7-11 well to create curves for LR ($\lambda\rho$) and MR ($\mu\rho$). Petrophysical cross-plots represent the log samples for the LR ($\lambda\rho$) and MR ($\mu\rho$) logs plotted against each other (figure 12). All points within the polygon in the cross-plot space are posted at the corresponding data points on the log curves. The petrophysical model supports the predicted results as the upper VTI layer of the shear zone has higher $\lambda\rho$ and low $\mu\rho$ than the lower HTI interval.
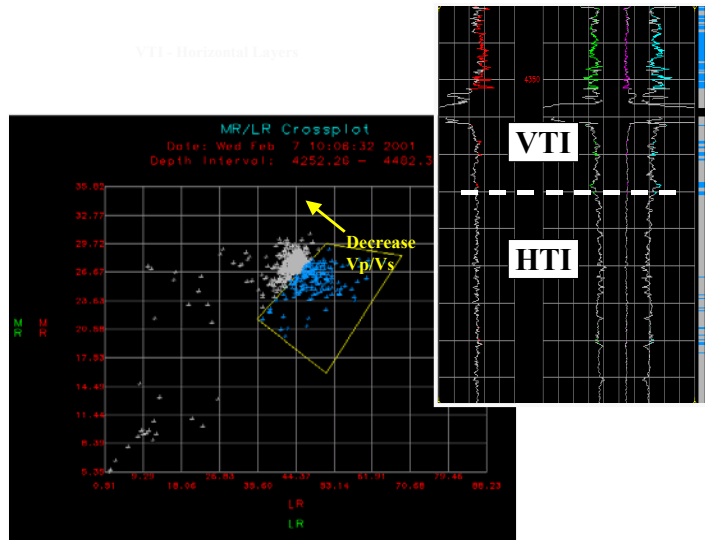
Fig. 12: LMR template (Petrophysical Crossplot). The sub-horizontal fractures of the VTI layer cross-plot as high $\lambda\rho$ and low $\mu\rho$ relative to the HTI layer.

Note that the posted values for the HTI interval are trending toward the direction of decreasing Vp/Vs ratio. Recall from figure 9 that the Vp/Vs ratio is higher when the shear waves are polarized across the HTI fractures. Of course information from that polarization direction is not represented in this log crossplot. It would be very challenging to derive a reliable log of S2 velocity from the full waveform data.

A similar crossplot method is employed to evaluate the seismic LMR response. The following figure is a crossplot of the LR ($\lambda\rho$) and MR ($\mu\rho$) data extracted from the surface seismic near the well location (using the method of Goodway et al.). The line selected for LMR processing is oriented oblique to the fault plane and as a result contains AVO information from an azimuth neither along strike or dip of the fractures. The points in the "crossplot space" represent all the samples of the two volumes plotted against each other. The crossplot points in high $\lambda\rho$ and low $\mu\rho$ correspond to the VTI layer in the upper segment of the log range. The crossplot points in lower $\lambda\rho$ and higher $\mu\rho$ correspond to the HTI layer in the centre of the log range. The rest of the points fall into the background of the crossplot space, beneath and outside the reservoir.
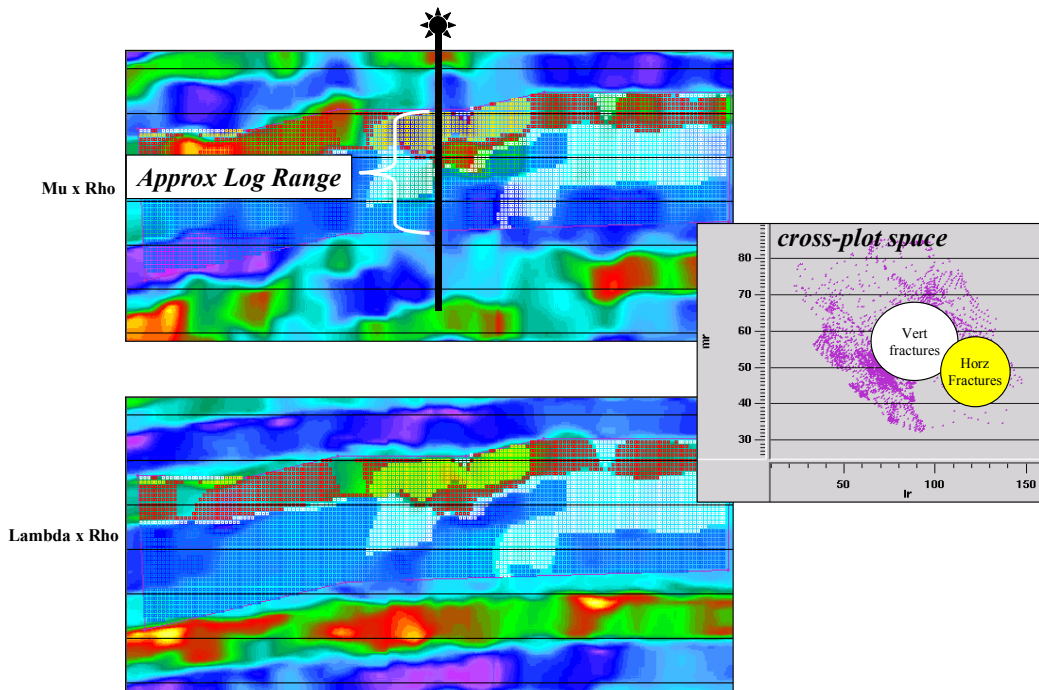
Fig. 13: Surface seismic LMR example. The sub-horizontal fractures shear zone (yellow) has high $\lambda\rho$ and low $\mu\rho$ relative to the sub-vertical tension fractures (white) near the fault plane. This observed LMR response matches that which was predicted for VTI and HTI in the petrophysical LMR template from the 7-11 well logs.

Conclusions

The difference in reflection amplitude between the conventional and swath data was caused by azimuthal anisotropy. It is proposed that shear wave splitting, observed in the full waveform sonic data of the HTI layer, is the dominant cause of the observed anisotropy. The azimuthal AVO trends predicted by the Ruger (1998) expression satisfy the observed trends on the CMP gathers. Although there is no disagreement with the predicted AVO, there is still some uncertainty in the observed AVO along fracture strike because of the offset limitation of the swath data.

With a more complete data set, perhaps a 3D survey, a map of amplitude derived from data oriented along the fracture symmetry axis could be used to map the extent of the HTI layer. This would impact the ability to predict fracture density, estimate reserves, facilitate future development or identify new prospects.

The secondary focus of the study was to test the potential for LMR analysis in this obviously anisotropic environment. Although the expected benefit was uncertain at the onset of the study, it generated surprisingly effective results and

13

separated the VTI from HTI media as predicted. LMR is a powerful tool if the interpreter is conscious of the limitations of the model on which it is based.

References

Ruger, A., 1998, Variations of P-wave reflectivity with offset and azimuth in anisotropic media: *Geophysics* **63**, 935-947

Thomsen, L., 1986, Weak elastic anisotropy: *Geophysics* 51, 1954-1966

Thomsen, L., 2002, Understanding Anisotropy in Exploration and Exploitation: SEG EAGE Distinguished instructor short course notes, series 86-0, volume112-3, p3-21

Goodway, B., 2001, AVO and Lame Constants for Rock Parameterization and Fluid Detection: CSEG Recorder, vol 26, p39

Ruger, A. &Tsvankin, I., 1997, Using AVO for fracture detection: Analytic basis and practical solutions: The Leading Edge, 16, no.10m 1429-1434

Shen, F., Sierra, J., Burns, D.R. & Toksuz, M.N, 2002b, Effects of fractures on NMO velocities and P-wave azimuthal AVO response: Geophysics